Buckling transitions of a beam at a stagnation point

By L. Guglielmini, A. Kushwaha, E. Shaqfeh AND H. A. Stone

1. Motivation and objectives

The interplay between viscous and elastic stresses is relevant to a large number of flow problems involving deformable bodies in a flow; slender elastic fibers in a viscous flow field are an example. In particular, in the low-Reynolds-number regime elastodynamics is critical to understanding how microorganisms swim by wave propagations along an elastic flagellum (Goldstein & Langer 1995) or by the motion of an elastic filament driven at its base (Wiggins *et al.* 1998; Koehler & Powers 2000; Coq *et al.* 2008). Arrays of cilia perform a variety of functions in the human body by virtue of their rapid beating and the resulting flow generation; these include clearance of the protective airway surface liquid in the lungs (Smith *et al.* 2008a), establishment of left/right asymmetry in the developing embryo (Smith *et al.* 2008b; Cartwright *et al.* 2007), the transport of gametes and embryos in the reproductive tract (Fauci & Dillon 2006).

Recent experiments have demonstrated the formation of biofilm streamers in curved microchannels, filaments of bacteria and polymer which develop in the flow, at the middle plane of the channel, right after each turn, and following the accumulation of biofilms at the walls (Rusconi *et al.* 2010). In particular, filaments were shown to form in a region of weak but continuous extensional flow due to the presence of a secondary vortical flow at the corner.

Other interesting applications involve the deformation and migration of flexible fibers freely suspended in a flow, which may give rise to oriented phases or network structures (Kharchenko *et al.* 2003), or the dynamics of nanocarpets, high-density collection of nanotubes, which can be employed for flow or force sensing or to produce super hydrophobic substrates. It has been shown in experiments involving a suspension of microscopic fibers that there is a sharp transition from zero to positive first normal stresses as a consequence of the buckling induced in the fibers.

We consider here the simple problem of an elastic slender filament immersed in a viscous fluid and tethered at a stagnation point. The filament is initially aligned with the compression axis of the flow and may buckle and undergo complex dynamics as a result of the interplay between external viscous forces and elastic forces in the filament. Buckling of elastic slender filaments has been discussed previously for the case of free filaments in shear flow (Becker & Shelley 2001) and in cellular flow (Young & Shelley 2007; Wandersman *et al.* 2010), and a bifurcation to shape instabilities has been shown due to compression by the flow. Baczynski *et al.* (2007) discussed instead the buckling instability of a filament under compressive load in a two-spatial dimension and in the presence of thermal fluctuation, and showed that thermal fluctuations lead to the stretching of a buckled filament, whereas they compress unbuckled filaments. Other works have been dedicated to the study of filaments tethered to a surface (Pozrikidis 2011) or held in the flow at one end (Autrusson *et al.* 2011). Moreover, with reference to the particular flow configuration that we consider, Beck & Shaqfeh (2006) studied the dynamics of

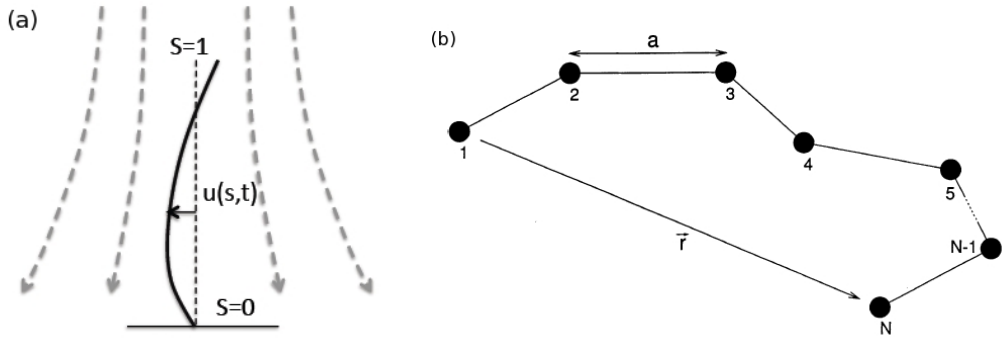

FIGURE 1. (a) Scheme of the problem we want to address, a filament immersed in a viscous extensional flow initially aligned with the compression axis of the flow. The filament position is described by the curvilinear coordinate s, and in the linear stability analysis we describe the evolution of the displacement with respect to the initial position $u(s,t)$. (b) Freely jointed bead-rod chain (Kramers chain) model for a polymer chain, constituted by N beads and $N-1$ rods of length a.

long-chain polymer molecules tethered to a plane wall and subject to a stagnation point flow. The polymer in this case is aligned with the elongation axis of the flow and initially coiled; a chain conformational hysteresis is shown to occur between the coiled and the stretched state.

In section 2 we describe a model for an elastic inextensible filament in a viscous flow and discuss the linear stability of a rod aligned initially with the compression axis of the extensional flow. We then introduce the bead-rod chain model (section 3), appropriate for semi-flexible polymers, that we used to simulate the complete, non-linear problem. Finally, in section 4 we outline a weakly non-linear stability approach, which enabled us to identify the Landau equation for the evolution of small perturbations in the neighborhood of transition points.

2. Continuum model for an elastic filament

We consider a slender, inextensible and elastic filament suspended in a viscous two-dimensional flow. We assume external forces, such as gravity, and Brownian forces to be negligible with respect to elastic and viscous forces. We also hypothesize inertial effects to be small, so that fluid motion is governed by the Stokes equations. Under these conditions, the filament is characterized by the aspect ratio R/L, where R and L are, respectively, the radius and the length of the filament, by the area moment of inertia I and by Young's modulus E. Let $\mathbf{x}(s,t)$ be the dimensionless position vector of the filament centerline in a cartesian reference frame, where s is the filament arclength and t the dimensionless time. The viscous force per unit length exerted on the filament by the undisturbed velocity field $\mathbf{U}_\infty$ can be expressed via the slender-body theory (Cox 1970), whereas filament forces consist of a bending and a tensile contribution and can be expressed via the Euler-Bernoulli equation. The dimensionless equation that describes our system reads (Autrusson *et al.* 2011)

$$\frac{\eta}{2}(2\mathbf{I} - \mathbf{x}_s^T\mathbf{x}_s)\cdot(\mathbf{U}_\infty - \mathbf{x}_t) = \mathbf{x}_{ssss} - (T(s,t)\mathbf{x}_s)_s\,, \tag{2.1}$$

where $T(s,t)$ is the tension in the filament and η represents the ratio of the viscous forces to the elastic forces and characterizes the behavior of an elastic thread immersed in a

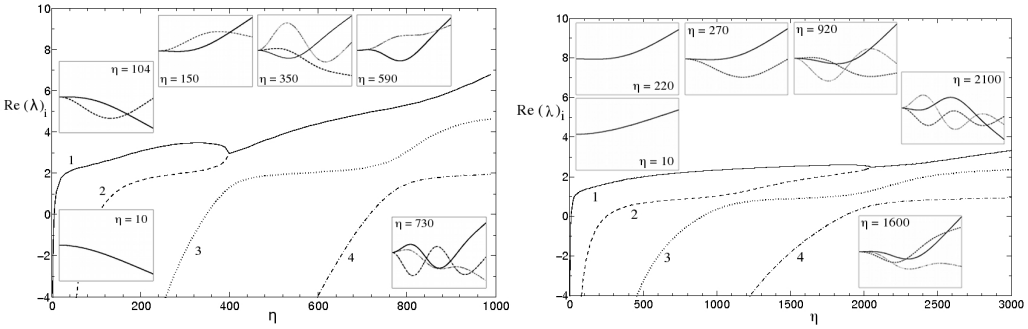

FIGURE 2. (a) For the linear flow configuration, the behavior of the first four eigenvalues of the problem 2.3 for increasing values of the parameter η. (b) For the quadratic flow configuration, the behavior of the first four eigenvalues of the problem 2.4 for increasing values of the parameter η. In the insets, the shape of the unstable eigenfunctions over the domain $s \in [0, 1]$ for various values of η. Note that the same line convention is used for each eigenfunction as for the corresponding eigenvalue.

viscous flow

$$\eta = \frac{4\pi\mu U_0 L^3}{EI \ln(L/R)}\,. \tag{2.2}$$

The constraint of inextensibility, which can be expressed as $\mathbf{x}_s \cdot \mathbf{x}_s = 1$, provides a further condition to be satisfied and yields a second-order boundary value problem for the line tension $T(s,t)$ (by deriving 2.1 with respect to s and operating a scalar product with $\mathbf{x}_s$). Moreover, we consider a thread that is held at one end and free at the other end (see Figure 1a). At the free end, $s = 1$, we require zero force and zero torque, which can be expressed as $\mathbf{x}_{ss} = \mathbf{x}_{sss} = \mathbf{0}$ and $T(s = 1, t) = 0$. At the fixed end, $s = 0$, the filament is clamped so that the position $\mathbf{x}(s = 0, t)$ and the slope $\mathbf{x}_s(s = 0, t)$ of the filament are constant, i.e., a force of constant orientation is applied at the constraint.

2.1. *Linear theory*

We want to study the linear stability of a filament immersed in a planar extensional flow field $\mathbf{U}_\infty = \{(x, -y), (xy, -y^2/2)\}$, held at the stagnation point $\mathbf{x}^0$ and initially lying at the straight equilibrium position (Figure 1a). We follow the approach proposed by Becker & Shelley (2001) for a buckling filament in a shear flow, where, for the flow geometry considered here, the unperturbed shape of the filament is not a function of time. The position of the filament is specified as $\mathbf{x} = \mathbf{x}^0 + s\,\mathbf{e}_2 + u(s,t)\,\mathbf{e}_1$, where $\mathbf{x}^0$ is the base of the filament, constant in time, and $u(s,t)$ is the deflection relative to the straight rod. Thus $u(s = 0, t) = 0$ and $u_s(s = 0, t) = 0$. Moreover, we express the velocity field as $\mathbf{U}_\infty(\mathbf{x}) = \mathbf{U}_\infty(\mathbf{x}^0) + \mathbf{x} \cdot \nabla\mathbf{U}_\infty(\mathbf{x}^0) + \mathbf{x} \cdot H(\mathbf{U}_\infty(\mathbf{x}^0)) \cdot \mathbf{x}/2$. We linearize Eq. 2.1 for small deflections $|u| \ll 1$ and the two velocity distributions. For the linear extensional flow $\mathbf{U}_\infty = (x, -y)$, the tension distribution and the evolution equation for the filament deflection are

$$T(s,t) = (s^2 - 1)\frac{\eta}{4}\,, \qquad u_t = u + s u_s + (s^2 - 1)\frac{u_{ss}}{4} - \frac{1}{\eta}u_{ssss}\,. \tag{2.3}$$

For the quadratic extensional flow $\mathbf{U}_\infty = (xy, -y^2/2)$, we get

$$T(s,t) = (s^3 - 1)\frac{\eta}{12}\,, \qquad u_t = su + \frac{s^2}{2}u_s + (s^3 - 1)\frac{u_{ss}}{12} - \frac{1}{\eta}u_{ssss}\,. \tag{2.4}$$

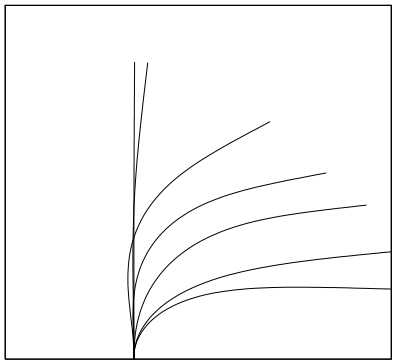

FIGURE 3. Example of the transient experienced by a filament in the quadratic extensional flow, from a straight position to the bent equilibrium configuration. In this case $\eta = 400$.

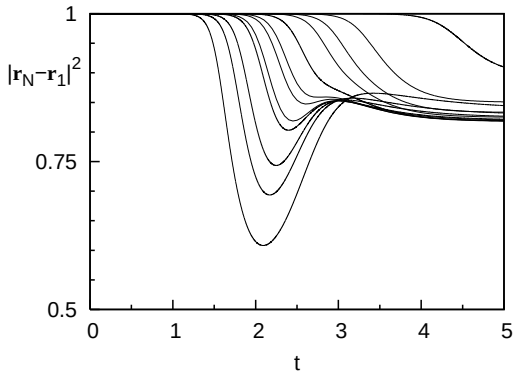

FIGURE 4. End-to-end length of the filament, defined as $|\mathbf{r}_N - \mathbf{r}_i|$, versus time, for decreasing values of η and increasing values of the persistence length l_p (corresponding curves are found moving in the plot from left to right).

We discuss the filament instability to in-plane disturbances of the form $u(s,t) = u(s)\mathrm{e}^{\lambda t}$, subject to appropriate boundary conditions. Pseudospectral collocation, using the Galerkin-type Chebyshev expansion $u(s) = \sum_{n=0}^{N} a_n \Phi_n$ with $\Phi_n = (\lambda^2 - 1/4)T_n(2s-1)$, yields a generalized matrix eigenvalue problem for the mode amplitudes a_n with eigenvalue λ.

Figure 2 shows the behavior of the first four eigenvalues of the problem for increasing values of the parameter η. For the case of a linear extensional flow, with the filament held at the position of vanishing velocity, we find a first critical value for $\eta = 5.25$, at which the first "bending" mode becomes unstable, and a second critical value for $\eta = 103$, at which a second "buckling" mode becomes unstable. For a quadratic extensional flow, which represents the realistic situation of a filament at a wall stagnation point, the real part of the eigenvalue which corresponds to the "bending" mode is positive for $\eta = 9$, while a second positive eigenvalue, corresponding to the buckling mode, appears for $\eta = 250$. In both panels, insets show the unstable eigenfunctions for various values of η. We can observe that as η increases the shape of eigenfunctions changes, so that, for example, the first eigenfunction initially describes "bending", while for larger values of η a point of relative minimum appears in its shape (for $\eta = 130$ and $\eta = 170$, respectively) and it turns into a "buckling" mode (a further point of maximum appears for $\eta = 590$ and $\eta = 900$, respectively). Also, the first eigenvalue remains the eigenvalue with largest real part over the range of values of η considered. Finally, we observe that for both the linear and the quadratic flows, at some point the first two eigenfunctions (and eigenvalues) get closer and closer until the eigenvalues and the corresponding eigenfunctions become complex, with the same real parts and conjugate imaginary parts ($\eta = 400$ and $\eta = 2060$, respectively).

3. Numerical method: a bead-rod chain model

In order to verify the validity of our linear theory, we decided to numerically solve the fully non-linear problem by means of a bead-rod chain model appropriate for semi-flexible polymers in a viscous flow. The semi-flexible polymer chain is represented by a bead-rod chain consisting of N beads connected by $N-1$ rigid rods of length a (Figure

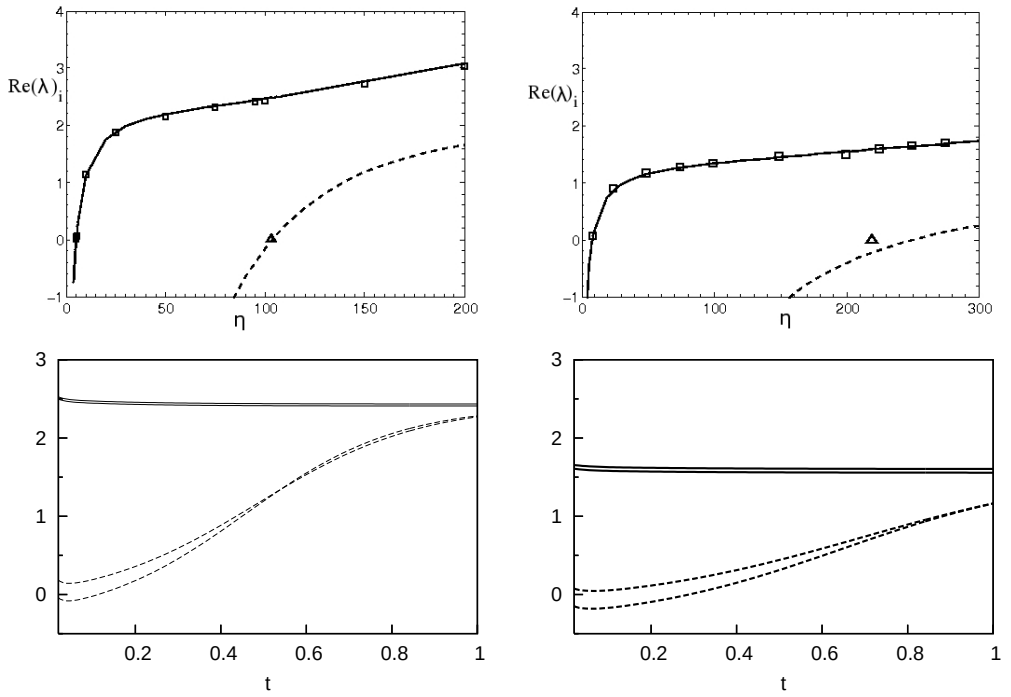

FIGURE 5. Comparison between results from linear stability analysis and numerical simulations, for the flows $U = (x, -y)$ (left column) and $U = (xy, -y^2/2)$ (right column). Plots in the first row show the behavior of the first two eigenvalues for increasing η, where lines refer to linear stability and markers represent numerical results. Plots in the second row show the curves of $\dot{a}_1/a_1$ (continuous line) and $\dot{a}_2/a_2$ (dashed line) versus time for two values of η chosen slightly smaller and larger than the critical value of η for buckling ($\eta = 95$ and 100 for the linear flow, $\eta = 200$ and 225 for the quadratic flow).

1b). The beads serve as interaction points with the solvent, whereas the massless rods act as rigid constraints in the chain and keep every bead at a constant distance away from its neighboring beads. Since we are interested in the chain dynamics under flow and in proximity of a wall, it is appropriate to use a modified version of the Kramers freely-jointed bead-rod chain model (Kramers 1956) that includes the bending modulus, i.e., the Kratky-Porod model (Kratky & Porod 1949; Lueth & Shaqfeh 2007). In this model the chain has more segments than Kuhn steps, so that it is possible to allow the bending modulus to control the persistence length regardless of the discretization of the chain (Ottinger 1996). The governing equations for the dynamics of the chain are obtained by summing the external forces acting on the beads:

$$F_i^H + F_i^T + F_i^C + F_i^W + F_i^B = 0\,, \qquad i = 1, 2, ..., N\,, \tag{3.1}$$

where the subscript i refers to the bead number and F_H, F_T, F_C, F_W, F_B are, respectively, the hydrodynamic drag force, the constraint force, the bending force, the wall force and the Brownian force. The hydrodynamic force is generally written as the drag acting on the bead in the absence of hydrodynamic interactions and fluid inertia,

$$F_i^H = -\zeta(\dot{\mathbf{r}}_i - \mathbf{U}_i^\infty)\,, \tag{3.2}$$

where $\dot{\mathbf{r}}_i$ is the velocity of the bead, $\mathbf{U}_i^\infty$ is the solvent velocity at the bead i position, and ζ is the drag coefficient. For this specific problem we chose the drag coefficient as the non-isotropic leading order term for a cylindrical shape of aspect ratio $\epsilon = R/L \ll 1$ from slender-body theory (Cox 1970). The constraint force keeps two neighboring beads at a constant distance a from each other, and can be written in terms of the tensions T_i in the rods as follows,

$$F_i^T = T_i \mathbf{q}_i - T_{i-1}\mathbf{q}_{i-1}\,, \tag{3.3}$$

where $\mathbf{q}_i = (\mathbf{r}_{i+1} - \mathbf{r}_i)/a$ is the orientation of the rod i connecting beads i and $i+1$ at positions $\mathbf{r}_i$ and $\mathbf{r}_{i+1}$, respectively. The bending force is obtained by evaluating the first variation of the bending energy of a semi-flexible polymer (Harris & Hearst 1966)

$$F_i^C = \hat{l}_p a k_B \mathcal{T} \kappa''\,, \tag{3.4}$$

where $\hat{l}_p$ is is the persistence length of the chain, $\mathcal{T}$ is the temperature and κ the local curvature of the chain, which is discretized in terms of the beads positions $\mathbf{r}_i$. The wall exclusion force is a non-physical interaction which prevents the beads from penetrating the wall, is in general very large close to the wall, has a very short range of influence and can be expressed with various formulas, which we don't list here for the sake of brevity (Lueth & Shaqfeh 2007). Finally, the Brownian force represents the frequent collisions between the beads and the solvent molecules and is mathematically modeled as a quantity with zero mean and a second moment that balances the dissipative forces (Ottinger 1996). After substitution of the different forces acting on the beads into Eq. (3.1) and rearranging, one can obtain the following set of equations governing the evolution of the position vectors:

$$d\mathbf{r}_i = \mathbf{u}_i^\infty + (\frac{F_i^T + F_i^C + F_i^W}{\zeta})dt + \sqrt{\frac{2k_B\mathcal{T}}{\zeta}}d\mathbf{W}_i\,, \qquad i = 1, 2, ..., N\,, \tag{3.5}$$

where $d\mathbf{W}_i$ is a Weiner process, i.e., a Gaussian random number with zero mean and variance dt. Further, the constraint that the separation between adjacent beads has to remain equal to a needs to be enforced. A system of $2N-1$ equations for N position variables $\mathbf{r}_i$ and $N-1$ tensions T_i is identified and solved with a predictor-corrector scheme for the position equation and LU factorization for the equation for the tension. In the final formulation of the governing equations, the distance between adjacent beads a serves as the length scale, the bead diffusion time $\zeta a^2/k_BT$ serves as the characteristic time scale and the forces are made dimensionless with $k_B\mathcal{T}/a$. Two dimensionless parameters appear, namely, the dimensionless persistence length $l_p = \hat{l}_p/a$ and the Peclet number, defined as the ratio between the convective and the diffusive time scales, $Pe = \dot{\gamma}(\zeta a^2/k_B\mathcal{T})$ with $\dot{\gamma}$ the shear rate.

3.1. *Results*

Figure 3 shows a typical solution for a buckling filament at a wall stagnation point ($\eta = 400$) at various time instants during the transient from its initial straight position and its final equilibrium "bent" position. Figure 4 shows again for the quadratic extensional flow, the evolution of the filament end-to-end length in time for various values of the compliance η. We note that for a bending filament the end-to-end length is a decreasing function of time, while for a buckling filament the end-to-end length displays a point of minimum or a flex at a certain time. The most appropriate way to compare numerical solutions with results from stability analysis is to expand the position of the filament

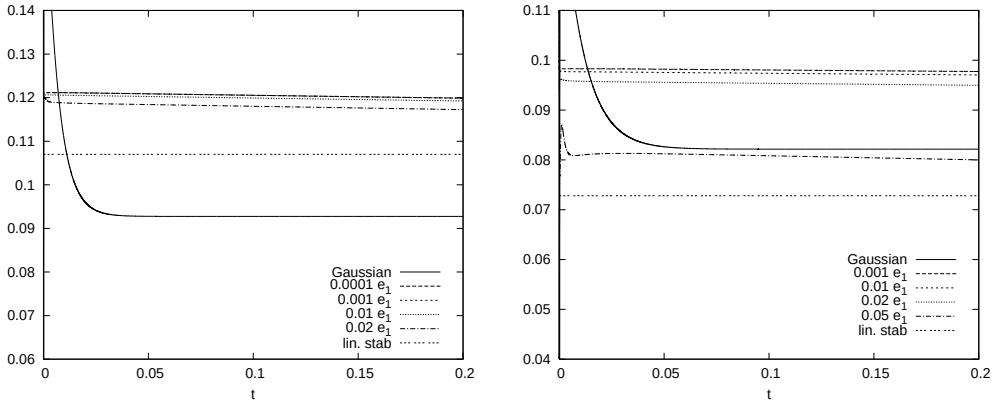

FIGURE 6. Behavior of the filament in a linear extensional flow (left plot) and in a quadratic extensional flow (right plot) when an initial perturbation of increasing amplitude is applied and for a value of $\eta = \eta_c + \Delta\eta$, with $\Delta\eta/\eta \simeq \epsilon^2$, $\epsilon = 0.2$ and η_c the critical point for bending. The ratio $\dot{a}_1/a_1$ is plotted versus time for a Gaussian small initial perturbation and for a perturbation proportional to the first eigenvalue e_1 of increasing amplitude. The value of the first eigenvalue λ_1 is also reported.

$y(s,t)$ at each time on the base formed by the eigenfunctions $e_i(s)$ of problems (2.3) or (2.4). We have in fact $y(s,t) = \sum a_i(t)e_i(s)$, with $a_i(t) = \langle e_i^\dagger(s), y(s,t)\rangle$, where $e_i^\dagger(s)$ are the eigenfunctions of the adjoint problem associated with each of (2.3) or (2.4). This allows us to directly compare results from linear stability and numerical simulations (Figure 5 top row), providing good agreement between the two approaches for both the flow configurations. The bottom row diagrams in Figure 5 show the behavior of the ratios $\dot{a}_1/a_1$ and $\dot{a}_2/a_2$ as function of time for two values of η chosen slightly smaller and larger than the critical value of η for buckling ($\eta = 95$ and 100 for the linear flow, $\eta = 200$ and 225 for the quadratic flow). We note that while $\dot{a}_1/a_1$ remains constant during the transient and equal to the value of λ_1 as found from linear stability, $\dot{a}_2/a_2$ grows with time and at the beginning of the transient displays a minimum which matches the value of λ_2 (in this case $\lambda_2 \sim 0$ since we chose values of η very close to η_c).

4. Weakly non-linear theory

In order to better characterize the bifurcation points identified by linear stability, we have developed a weakly non-linear perturbative approach. We expand the functions describing the position and the tension of the filament as

$$\mathbf{x}(s,\tau) = \{\epsilon u^1 + \epsilon^2 u^2 + \epsilon^3 u^3, s + \epsilon(\epsilon v^1 + \epsilon^2 v^2)\}\,, \qquad T(s,\tau) = T^0 + \epsilon T^1 + \epsilon^2 T^2\,, \quad (4.1)$$

where $u^1(s,\tau) = A(\tau)U^1(s)$, and $U^1(s)$ is the eigenfunction corresponding to the eigenvector whose real part vanishes at the critical point considered. We introduced slow time scale τ such that $\tau = \epsilon^2 t$. We anticipate that, for symmetry reasons, the amplitude equation for A will be invariant to a change of sign of A and therefore the nonlinear term of lowest power of A will be cubic. Also, the rate of the initial exponential growth of the amplitude of u^1, hence the eigenvalue, will have to be of order ϵ^2, and therefore $(\eta - \eta_c)/\eta = \Delta\eta/\eta = O(\epsilon^2)$. We rewrite Eq. 2.1 so that the smaller terms are on the

right-hand side,

$$\frac{\eta_c}{2}(2\mathbf{I}-\mathbf{x}_s^T\mathbf{x}_s)\cdot\mathbf{U}_\infty-(\mathbf{x}_{ssss}-T(s,t)\mathbf{x}_s)_s=\frac{\eta_c}{2}(2\mathbf{I}-\mathbf{x}_s^T\mathbf{x}_s)\cdot\mathbf{x}_t+\frac{1-R}{R}(\mathbf{x}_{ssss}-T(s,t)\mathbf{x}_s)_s)\,, \tag{4.2}$$

where $R=\eta/\eta_c$. A further equation is provided by the inextensibility condition $\mathbf{x}_s\cdot\mathbf{x}_s=1$. Eq. 4.2 and the inextensibility condition are expanded using the definitions in Eq. 4.1. For brevity, we only list results for the linear extensional flow field. At the zero and first order in ϵ we recover the same problem from linear theory and the same solutions for T^0 and U^1. Moreover, we have $T^1=0$. At order ϵ^2 and ϵ^3 we write the following equations in u^2, v^1, u^3, T^2 :

$$\eta_c(u^2+su_s^2+\frac{(s^2-1)}{4}u_{ss}^2)-u_{ssss}^2=0\,, \tag{4.3}$$

$$\eta_c(-\frac{v^1}{2}+\frac{3}{2}sv_s^1+\frac{(s^2-1)}{4}v_{ss}^1)-v_{ssss}^1-\frac{\eta_c}{2}u^1u_s^1+T_s^2=\frac{R-1}{2R}s\,, \tag{4.4}$$

$$u_s^1u_s^1+2v_s^1=0\,, \tag{4.5}$$

$$\eta_c(u^3+su_s^3+\frac{(s^2-1)}{4}u_{ss}^3)-u_{ssss}^3+(T^2u_s^1)_s+ \tag{4.6}$$
$$\frac{\eta_c}{2}(v^1u_s^1+sv_s^1u_s^1-u^1(u_s^1)^2)=$$
$$\eta_cu_\tau^1-\frac{1-R}{R}(\eta_c\frac{s}{2}u_s^1+\eta_c\frac{(s^2-1)}{4}u_{ss}^1-u_{ssss}^1)\,,$$

We immediately see that $u^2=0$, while solutions for v^1 and T^2 can be found by solving Eq. 4.4, 4.5 with the boundary conditions $T^2(s=1)=0$, $v^1(s=0), v_s^1(s=0)=0$, $v_{ss}^1(s=1)=v_{sss}^1(s=1)=0$ and observing that from the structure of equations it follows that:

$$v^1(s,\tau)=A^2(\tau)V^1(s)\,,\quad T^2(s)=\eta_c\frac{R-1}{R}\frac{(s^2-1)}{4}+A^2(\tau)K^2(s)\,. \tag{4.7}$$

We observe that the equation at order ϵ^3 (4.7) has the shape $Lu^3=G$, where L is the linear operator characterizing Eq. 2.3, 4.7. We seek the adjoint operator $L^\dagger$ of L, with appropriate boundary conditions $B^\dagger$ of B, and find all the solutions of the adjoint problem $L^\dagger u^\dagger=0$, $B^\dagger=0$. Finally, we form the inner product $\langle G,u^\dagger\rangle$ and obtain a solvability condition which also provides the evolution equation for $A(\tau)$ (Landau equation)

$$\eta_cU^1\frac{dA}{d\tau}=\frac{R-1}{R}U_{ssss}^1A(\tau)+ \tag{4.8}$$
$$\left[\frac{\eta_c}{2}(V^1U_s^1+sV_s^1U_s^1-U^1(U_s^1)^2)+(K^2U_s^1)_s\right]A^3(\tau)\,.$$

For the linear extensional flow configuration at the first ($\eta=5.25$) and second ($\eta=103.7$) critical points, for $\Delta\eta/\eta\sim O(\epsilon^2)$ and $\epsilon=0.2$, the Landau equation reads

$$A'(\tau)=0.107A(\tau)+0.05A^3(\tau)\,. \tag{4.9}$$

$$A'(\tau)=0.167A(\tau)+28.2A^3(\tau)\,. \tag{4.10}$$

For the quadratic extensional flow configuration at the first ($\eta=9.2$) and second ($\eta=250$) critical points, for $\Delta\eta/\eta\sim O(\epsilon^2)$ and $\epsilon=0.2$, the Landau equation reads

$$A'(\tau)=0.063A(\tau)-3.07A(\tau)^3\,. \tag{4.11}$$

$$A'(\tau) = 0.0603454A(\tau) + 6.72823A(\tau)^3\,. \tag{4.12}$$

These results suggest, for the filament immersed in a quadratic extensional flow, supercritical stability for small $\Delta\eta > 0$ beyond the bending critical point, and subcritical instability around the buckling critical point. Both critical points display instead subcritical instability for a filament in the linear extensional flow. Preliminary results from numerical simulations for the first critical point in both flow configurations seem to show supercritical stability. In Figure 6 we report the behavior of the filament in a linear and quadratic extensional flow for a value for η very close to the first critical point when an initial perturbation proportional to the first eigenfunction e_1 and of increasing amplitude is applied. We observe that the growth rate $\dot{a}_1$ of the disturbance decreases for increasing amplitude of the initial perturbation $a_1(\tau = 0)$, proportionally to the third power of the amplitude, as suggested by the Landau equation. However, numerical solutions very close to the transition point also present a significant dependence on the shape of the initial condition, a behavior which might be indicative of subcriticality. We plan to study further the numerical solution of the complete problem in the neighborhood of the critical points in order to better characterize bifurcations.

5. Conclusion and future work

In conclusion, we have developed a linear stability analysis of the problem of an elastic inextensible filament in a two-dimensional extensional flow and initially aligned with the compression axis of the filament. We have identified the critical value of the dimensionless compliance η, comparing viscous forces and elastic forces, which leads to bending and buckling instability, for both a linear extensional flow and a quadratic extensional flow (flow in the vicinity of a wall stagnation point). We have performed direct numerical simulations for the complete non-linear problem and we have expanded results for the position of the filament on the base of the eigenfuctions in order to directly compare and verify results from linear stability. Finally, we have developed a weakly-nonlinear analysis, which seems to suggest subcritical instability for the bucking transition in both flows and for the bending transition in the linear flow, supercritical stability for the bending transition for a filament in a quadratic extensional flow. We plan to study further by numerical simulations the dependence of our dynamic system on initial perturbations and to characterize the identified bifurcation. We will also be looking into the effect of thermal fluctuations in order to verify whether the behavior described in Baczynski *et al.* (2007) also applies to our problem. The numerical model should also enable us to discuss how the flexibility of the filament modifies the rheology of the fluid in the neighborhood of the wall by contributing to its bulk stress tensor.

REFERENCES

Autrusson, N., Guglielmini, L., Lecuyer, S., Rusconi, R. & Stone, H. A. 2011 The shape of an elastic filament in a two-dimensional corner flow. *Physics of Fluids* **23**, 99–99.

Baczynski, K., Lipowsky, R. & Kierfeld, J. 2007 Stretching of buckled filaments by thermal fluctuations. *Physical Review E* **76**, 061914.

Beck, V. & Shaqfeh, A. 2006 Ergodicity breaking and conformal hysteresis in the dynamics of a polymer tethered at a surface stagnation point. *The Journal of Chemical Physics* **124**, 094902.

Becker, L. & Shelley, M. 2001 Instability of elastic filaments in shear flow yields first-normal stress differences. *Physical Review Letters* p. 198301.

Cartwright, J. H. E., Piro, N. O. & Tuval, I. 2007 Embryonic nodal flow and the dynamics of nodal vesicular parcels. *Journal Royal Society Interface* **4**, 49–55.

Coq, N., du Roure, O., Marthelot, J., Bartolo, D. & Fermigier, H. 2008 Rotational dynamics of a soft filament: wrapping transition and propulsive forces. *Physics of Fluids* **20**, 051703.

Cox, R. G. 1970 The motion of long slender bodies in a viscous fluid, part 1. general theory. *Journal of Fluid Mechanics* **44**, 791–810.

Fauci, L. J. & Dillon, R. 2006 Biofluidmechanics of reproduction. *Annual Review of Fluid Mechanics* **38**, 371–394.

Goldstein, R. E. & Langer, S. A. 1995 Nonlinear dynamics of stiff polymers. *Physical Review Letters* **75**, 1094–1097.

Harris, R. A. & Hearst, J. E. 1966 On polymer dynamics. *The Journal of Chemical Physics* **44** (7), 2595–2602.

Kharchenko, S., Douglas, J., Obrzut, J., Grulke, E. & Migler, K. 2003 Fluid mechanics of nodal flow due to embryonic primary cilia. *Nature Materials* **3**, 564–568.

Koehler, S. A. & Powers, T. R. 2000 Twirling elastica: kinks, viscous drag, and torsional stress. *Physical Review Letters* **85**, 4827–4830.

Kramers, H. A. 1956 *Collected Scientific Papers*. North-Holland Puclishing Co.

Kratky, O. & Porod, G. 1949 Rontgenuntersuchung geloster fadenmolekule. *Recueil des Travaux Chimiques des Pays-Bas* **68**, 1106.

Lueth, C. A. & Shaqfeh, E. G. 2007 Tethered dna shear dynamics in the flow gradient plane: application to double tethering. *Korea-Australia Rheology Journal* **19**, 141–146.

Ottinger, H. C. 1996 *Stochastic Processes in polymer Fluids*. Springer.

Pozrikidis, C. 2011 Shear flow past slender elastic rods attached to a plane. *International Journal of Solids and Structures* **48**, 137–143.

Rusconi, R., Lecuyer, S., Guglielmini, L. & Stone, H. A. 2010 Laminar flow around corners triggers the formation of biofilm streamers. *Journal of the Royal Society Interface* **7**, 1293–1299.

Smith, D. J., Gaffney, E. & Blake, J. 2008a Modelling mucociliary clearance. *Respir. Physiol. Neurobiol.* **163**, 178–188.

Smith, D. J., Gaffney, E. & Blake, J. 2008b Fluid mechanics of nodal flow due to embryonic primary cilia. *International Journal of Solids and Structures* **5**, 567–573.

Wandersman, E., Quennouz, N., Fermigier, M., Lindner, A. & du Roure, O. 2010 Buckled in translation. *Soft Matter* **6**, 5715–5719.

Wiggins, C. H., Riveline, D., Ott, A. & Goldstein, R. E. 1998 Trapping and wiggling: elastohydrodynamics of driven microfilaments. *Biophysical Journal* **74**, 1043–1060.

Young, Y.-N. & Shelley, M. 2007 Stretch-coil transition and transport of fibers in cellulars flows. *Physical Review Letters* **99**, 058303.